NASA/TM—2007-214679

Orbit Determination Analysis Utilizing Radiometric and Laser Ranging Measurements for GPS Orbit

Bryan W. Welch
Glenn Research Center, Cleveland, Ohio

February 2007

NASA STI Program . . . in Profile

Since its founding, NASA has been dedicated to the advancement of aeronautics and space science. The NASA Scientific and Technical Information (STI) program plays a key part in helping NASA maintain this important role.

The NASA STI Program operates under the auspices of the Agency Chief Information Officer. It collects, organizes, provides for archiving, and disseminates NASA's STI. The NASA STI program provides access to the NASA Aeronautics and Space Database and its public interface, the NASA Technical Reports Server, thus providing one of the largest collections of aeronautical and space science STI in the world. Results are published in both non-NASA channels and by NASA in the NASA STI Report Series, which includes the following report types:

- TECHNICAL PUBLICATION. Reports of completed research or a major significant phase of research that present the results of NASA programs and include extensive data or theoretical analysis. Includes compilations of significant scientific and technical data and information deemed to be of continuing reference value. NASA counterpart of peer-reviewed formal professional papers but has less stringent limitations on manuscript length and extent of graphic presentations.

- TECHNICAL MEMORANDUM. Scientific and technical findings that are preliminary or of specialized interest, e.g., quick release reports, working papers, and bibliographies that contain minimal annotation. Does not contain extensive analysis.

- CONTRACTOR REPORT. Scientific and technical findings by NASA-sponsored contractors and grantees.

- CONFERENCE PUBLICATION. Collected papers from scientific and technical conferences, symposia, seminars, or other meetings sponsored or cosponsored by NASA.

- SPECIAL PUBLICATION. Scientific, technical, or historical information from NASA programs, projects, and missions, often concerned with subjects having substantial public interest.

- TECHNICAL TRANSLATION. English-language translations of foreign scientific and technical material pertinent to NASA's mission.

Specialized services also include creating custom thesauri, building customized databases, organizing and publishing research results.

For more information about the NASA STI program, see the following:

- Access the NASA STI program home page at *http://www.sti.nasa.gov*

- E-mail your question via the Internet to *help@sti.nasa.gov*

- Fax your question to the NASA STI Help Desk at 301–621–0134

- Telephone the NASA STI Help Desk at 301–621–0390

- Write to:
  NASA Center for AeroSpace Information (CASI)
  7115 Standard Drive
  Hanover, MD 21076–1320

NASA/TM—2007-214679

Orbit Determination Analysis Utilizing Radiometric and Laser Ranging Measurements for GPS Orbit

Bryan W. Welch
Glenn Research Center, Cleveland, Ohio

National Aeronautics and
Space Administration

Glenn Research Center
Cleveland, Ohio 44135

February 2007

Acknowledgments

I would like to thank the Space Communications Architecture Working Group for providing a forum to develop the orbit determination navigation analysis tools, and the opportunity to contribute to the analysis a comparison of utilizing radiometric versus radiometric/laser measurements for orbit determination of a GPS satellite orbit. I would also like to thank the Space Communication Data Systems Project for funding this effort.

This report contains preliminary findings, subject to revision as analysis proceeds.

Level of Review: This material has been technically reviewed by an expert single reviewer.

Available from

NASA Center for Aerospace Information
7115 Standard Drive
Hanover, MD 21076–1320

National Technical Information Service
5285 Port Royal Road
Springfield, VA 22161

Available electronically at http://gltrs.grc.nasa.gov

Orbit Determination Analysis Utilizing Radiometric and Laser Ranging Measurements for GPS Orbit

Bryan W. Welch
National Aeronautics and Space Administration
Glenn Research Center
Cleveland, Ohio 44135

Abstract

While navigation systems for the determination of the orbit of the Global Position System (GPS) have proven to be very effective, the current issues involve lowering the error in the GPS satellite ephemerides below their current level. In this document, the results of an orbit determination covariance assessment are provided. The analysis is intended to be the baseline orbit determination study comparing the benefits of adding laser ranging measurements from various numbers of ground stations. Results are shown for two starting longitude assumptions of the satellite location and for nine initial covariance cases for the GPS satellite state vector.

1. Introduction

The task of the laser ranging analysis effort is to determine the added benefits derived from solving for a spacecraft's state vector when utilizing laser ranging measurements in addition to the current use of pseudo-range and accumulated delta range (ADR), also known as Integrated Doppler measurements. The methodology to perform this analysis is to perform a covariance study for the Global Positioning System (GPS) orbit.

The first method will be to perform the orbit determination (OD) using pseudo-range and ADR measurements from the six Monitor Stations (MS) for the GPS satellite orbit through an Extended Kalman Filter (EKF) analysis. The second method will be to add laser ranging measurements from the six MS sites along with various amounts of additional sites. Measurements from both methods will be used to form estimates for the satellite's state vector, which will be propagated until new measurements are available. Finally, comparisons will be made between the performance of the current system and the modified system.

2. EKF Description

The purpose of an Extended Kalman Filter (EKF) is to estimate the states of a non-linear system. The EKF is an extension of the standard Kalman Filter, where its purpose is to estimate the states of a linear system. The derivation of the EKF is based on linearizing the non-linear system using the Kalman Filter estimate as the nominal state trajectory. The non-linear system is linearized around the Kalman Filter estimate and the Kalman Filter estimate is based on the linearized system (ref. 1).

The method of the EKF used for these simulations is the discrete time system/discrete time measurement EKF. This is the most appropriate method to simulate the EKF, as performing continuous time dynamics in a computer requires an extremely large amount of memory and processor power to be performed efficiently. Also, it is important to note up front that typically, there are multiple runs performed for each scenario. This is due to the fact that the equations of the EKF dictate that the real noise parameters, instead of the covariance of the noise (as in linear Kalman filter problems), be used to form new estimates of the state estimates. The following equations dictate the nature of the EKF process (ref. 1).

1) System and Measurement equations

$$x_k = f_{k-1}(x_{k-1}, u_{k-1}, w_{k-1}) \tag{1}$$

$$y_k = h_k(x_k, v_k) \tag{2}$$

$$w_k \rightarrow N(0, Q_k) \tag{3}$$

$$v_k \rightarrow N(0, R_k) \tag{4}$$

Where:

- f_k is the state equation at time k
- x_k is the state vector at time k
- u_k is the input vector at time k
- w_k is the state noise vector at time k
- h_k is the measurement equation at time k
- y_k is the measurement vector at time k
- v_k is the measurement noise vector at time k
- Q_k is the state noise covariance at time k
- R_k is the measurement noise covariance at time k

2) Filter Initial Conditions

$$\hat{x}_0^+ = E(x_0) \tag{5}$$

$$P_0^+ = E\left[(x_0 - \hat{x}_0^+)(x_0 - \hat{x}_0^+)^T\right] \tag{6}$$

Where:

- $E(\ )$ is the expectation operator
- $\hat{x}_0^+$ is the a posteriori state estimate at time 0
- P_0^+ is the a posteriori covariance estimate at time 0

3) Filter Loop

a) Compute the following partial derivative matrices

$$F_{k-1} = \frac{\partial f_{k-1}}{\partial x}\Big|_{\hat{x}_{k-1}^+} \tag{7}$$

$$L_{k-1} = \frac{\partial f_{k-1}}{\partial w}\Big|_{\hat{x}_{k-1}^+} \tag{8}$$

Where:

- $\frac{\partial f}{\partial x}|_{x_1}$ is the partial derivative operator of function f by vector x, evaluated by vector x_1
- F_k is the partial derivative matrix of the state equation by the state vector at time k
- L_k is the partial derivative matrix of the state equation by the state noise vector at time k

b) Perform the time update of the state estimate and estimation error covariance

$$P_k^- = F_{k-1} P_{k-1}^+ F_{k-1}^T + L_{k-1} Q_{k-1} L_{k-1}^T \tag{9}$$

$$\hat{x}_k^- = f_{k-1}\left(\hat{x}_{k-1}^+, u_{k-1}, 0\right) \tag{10}$$

Where:

- P_k^- is the a priori covariance estimate at time k
- $\hat{x}_k^-$ is the a priori state estimate at time k

c) Compute the following partial derivative matrices

$$H_k = \frac{\partial h_k}{\partial x}|_{\hat{x}_k^-} \tag{11}$$

$$M_k = \frac{\partial h_k}{\partial v}|_{\hat{x}_k^-} \tag{12}$$

Where:

- H_k is the partial derivative matrix of the measurement equation by the state vector at time k
- M_k is the partial derivative matrix of the measurement equation by the measurement noise vector at time k

d) Perform the measurement update of the state estimate and estimation error covariance

$$K_k = P_k^- H_k^T \left(H_k P_k^- H_k^T + M_k R_k M_k^T\right)^{-1} \tag{13}$$

$$\hat{x}_k^+ = \hat{x}_k^- + K_k\left[y_k - h_k\left(\hat{x}_k^-, 0\right)\right] \tag{14}$$

$$P_k^+ = \left(I - K_k H_k\right) P_k^- \tag{15}$$

Where:

- K_k is the Kalman gain matrix at time k
- $\hat{x}_k^+$ is the a posteriori state estimate at time k
- P_k^+ is the a posteriori covariance estimate at time k

3. State Dynamics Description

The orbit of a GPS satellite can be viewed as a simplified two-body problem. That is the assumption made for this analysis. Therefore, the differential equation that solves the two-body problem is as follows, in Eq. (16) (ref. 2).

$$\ddot{r} + \frac{\mu}{R^3} r = a_d \tag{16}$$

Where:

- r is the position matrix
- $\ddot{r}$ is the 2nd time derivative of the position matrix
- μ is the Earth's Gravitational constant
- R is the magnitude of the position matrix
- a_d is the orbital perturbation

It is important to note initially that the OD analysis solves for more than just the position matrix. The purpose of the OD analysis is to solve for position, velocity, clock bias, and frequency bias. Therefore, the state equation that governs the OD analysis is an extension of the two-body problem. Keep in consideration that the orbital perturbation is assumed to be zero for this analysis. The state is defined in Eq. (17), while the state equation is given as follows in Eq. (18).

$$x = \begin{bmatrix} r \\ v \\ ct_{bias} \\ c\dot{t}_{bias} \end{bmatrix} \tag{17}$$

$$\dot{x} = \begin{bmatrix} v \\ \frac{-\mu}{R^3} \\ 0 \\ 0 \end{bmatrix} x + \begin{bmatrix} 0 \\ 0 \\ 1 \\ 1/f \end{bmatrix} w \tag{18}$$

Where:

- r is the position matrix
- v is the velocity matrix
- c is the speed of light in a vacuum
- t_{bias} is the clock difference between the satellite and the ground stations
- f is the GPS L1 frequency
- w is the state noise

Equation (19) shows the fully expanded form of the discrete state equation. Equation (20) converts the state equation from Eq. (18) into a discrete time state equation, needed for the discrete time EKF, in Earth-Centered Fixed coordinates.

$$x_k = \begin{bmatrix} x_{k,1} \\ x_{k,2} \\ x_{k,3} \\ x_{k,4} \\ x_{k,5} \\ x_{k,6} \\ x_{k,7} \\ x_{k,8} \end{bmatrix} = \begin{bmatrix} r_{k,x} \\ r_{k,y} \\ r_{k,z} \\ v_{k,x} \\ v_{k,y} \\ v_{k,z} \\ ct_{bias} \\ \dot{ct}_{bias} \end{bmatrix} \tag{19}$$

$$x_{k+1} = \begin{bmatrix} \cos(\phi) & \sin(\phi) & 0 & \Delta\cos(\phi) & \Delta\sin(\phi) & 0 & 0 & 0 \\ -\sin(\phi) & \cos(\phi) & 0 & -\Delta\sin(\phi) & \Delta\cos(\phi) & 0 & 0 & 0 \\ 0 & 0 & 1 & 0 & 0 & \Delta & 0 & 0 \\ -\frac{\mu}{R^3}\cos(\phi) & -\frac{\mu}{R^3}\sin(\phi) & 0 & \cos(\phi) & \sin(\phi) & 0 & 0 & 0 \\ \frac{\mu}{R^3}\sin(\phi) & -\frac{\mu}{R^3}\cos(\phi) & 0 & -\sin(\phi) & \cos(\phi) & 0 & 0 & 0 \\ 0 & 0 & -\frac{\mu}{R^3} & 0 & 0 & 1 & 0 & 0 \\ 0 & 0 & 0 & 0 & 0 & 0 & 1 & 0 \\ 0 & 0 & 0 & 0 & 0 & 0 & 0 & 1 \end{bmatrix} x_k + \begin{bmatrix} 0 \\ 0 \\ 0 \\ 0 \\ 0 \\ 0 \\ 1 \\ 1/f \end{bmatrix} w_k \tag{20}$$

Where:

- ϕ is the Earth rotation rate in radians/second
- Δ is the discrete time step

4. Measurement Description

There are three different measurement types that are utilized within the trade space of this analysis. The first measurement is the pseudo-range (PR) measurement, which is utilized at the MS locations. The equation for the pseudo-range measurement is given in Eq. (21) (ref. 3).

$$PR = \sqrt{(x_1 - x_2)^2 + (y_1 - y_2)^2 + (z_1 - z_2)^2} + ct_{bias} + v_{PR} \tag{21}$$

Where:

- PR is the pseudo-range measurement
- (x_1, y_1, z_1) is the position of the transmitter (or receiver)
- (x_2, y_2, z_2) is the position of the receiver (or transmitter)
- v_{PR} is the noise term in the pseudo-range measurement

The second measurement type that is utilized at the six MS locations is the Accumulated Delta Range (*ADR*) measurement. This measurement also is called carrier phase. It is the integral of the range-rate measurement used with instantaneous Doppler shift. Equation (22) provides the mathematical description of the *ADR* measurement (ref. 3).

$$ADR = \sum_{k=0}^{n} \left(\frac{\left[\left(x_{1,k} - x_{2,k}\right)\left(vx_{1,k} - vx_{2,k}\right) + \left(y_{1,k} - y_{2,k}\right)\left(vy_{1,k} - vy_{2,k}\right) + \left(z_{1,k} - z_{2,k}\right)\left(vz_{1,k} - vz_{2,k}\right) \right]}{\sqrt{\left(x_{1,k} - x_{2,k}\right)^2 + \left(y_{1,k} - y_{2,k}\right)^2 + \left(z_{1,k} - z_{2,k}\right)^2}} + fc\dot{t}_{bias} + v_{ADR} \right) \quad (22)$$

Where:

- ADR is the accumulated delta range measurement
- $\left(vx_1, vy_1, vz_1\right)$ is the velocity of the transmitter (or receiver)
- $\left(vx_2, vy_2, vz_2\right)$ is the velocity of the receiver (or transmitter)
- v_{ADR} is the noise term in the accumulated delta range measurement

The final measurement type that is utilized only in the modified systems, but at all ground station sites, is the laser ranging (*LR*) measurement. This can be thought of as the equivalent of a two-way radiometric signal, in terms of the equation governing the measurement. Equation (23) provides the mathematical description of the *LR* measurement (ref. 3).

$$LR = \sqrt{\left(x_1 - x_2\right)^2 + \left(y_1 - y_2\right)^2 + \left(z_1 - z_2\right)^2} + v_{LR} \quad (23)$$

Where:

- LR is the laser ranging measurement
- v_{LR} is the noise term in the laser ranging measurement

Table 1 provides the standard deviation of the noise terms that are assumed for the three measurement equations provided in Eqs. (21) through (23).

TABLE 1.—STANDARD DEVIATION OF MEASUREMENT NOISE TERMS

Noise term	σ
v_{PR}	2 m
v_{ADR}	5 mm/s
v_{LR}	1m

5. Station Locations

The first of the two proposed systems that are analyzed is the current system, which utilizes pseudo-range and ADR measurements from the six MS locations. The second proposed system is the modified system, which utilizes all measurements for the current system, plus laser ranging measurements from the six MS locations along with measurements from various amounts of additional ground stations. The locations of the additional ground stations are from a listing of laser ranging sites from the International Laser Ranging Service (ref. 4). The six MS have their locations listed in table 2, below. Figure 1 illustrates the locations of the six MS sites, shown in red dots.

TABLE 2.—MS LOCATIONS

Station	Longitude (°E)	Latitude (°N)
Colorado Springs	–104.7167°	38.8167°
Hawaii	–158.2519°	21.5653°
Cape Canaveral	–80.5333°	28.4667°
Ascension Island	–14.3700°	–7.9500°
Diego Garcia	72.4000°	–6.5667°
Kwajalein	167.7319°	8.7189°

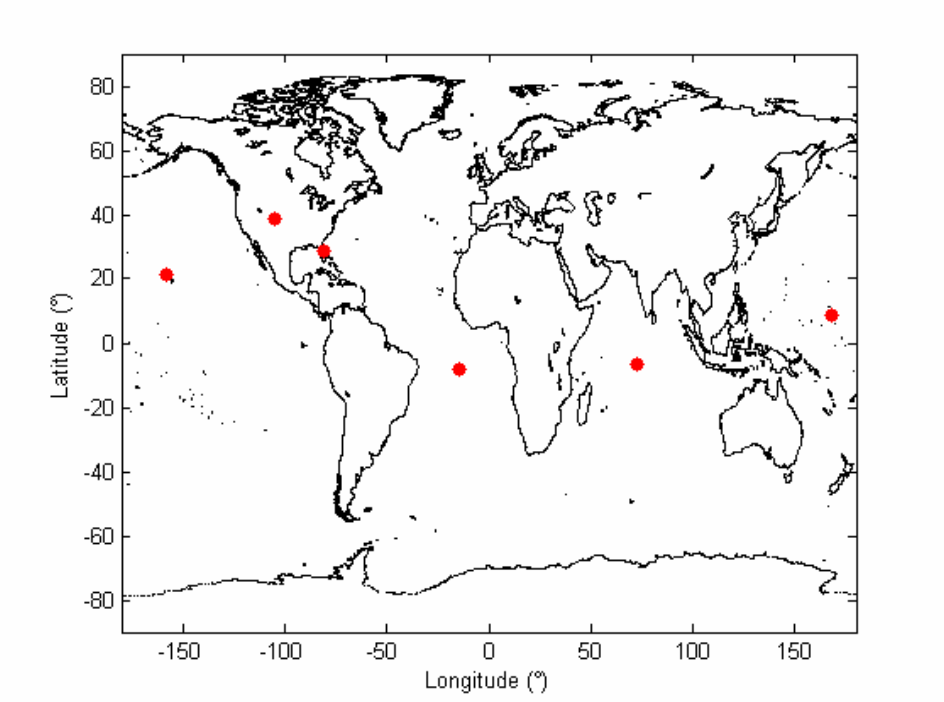

Figure 1.—Current system station map.

There are five modified system concepts. Modified System 1 (MSys1) utilizes all measurements from the current system plus laser ranging measurements from the six MS locations and two additional locations. Table 3 lists the locations for the two additional ground sites used for laser ranging measurements only for MSys1. Figure 2 illustrates the locations of the six MS and the two additional ground stations. The six MS are shown in red dots, while the two additional ground stations are shown in blue dots for the MSys1.

TABLE 3.—ADDITIONAL LASER RANGING STATION LOCATIONS—MSys1

Station	Longitude (°E)	Latitude (°N)
GSFC	–76.8760°	39.0044°
McDonald Observatory	–104.0217°	30.6717°

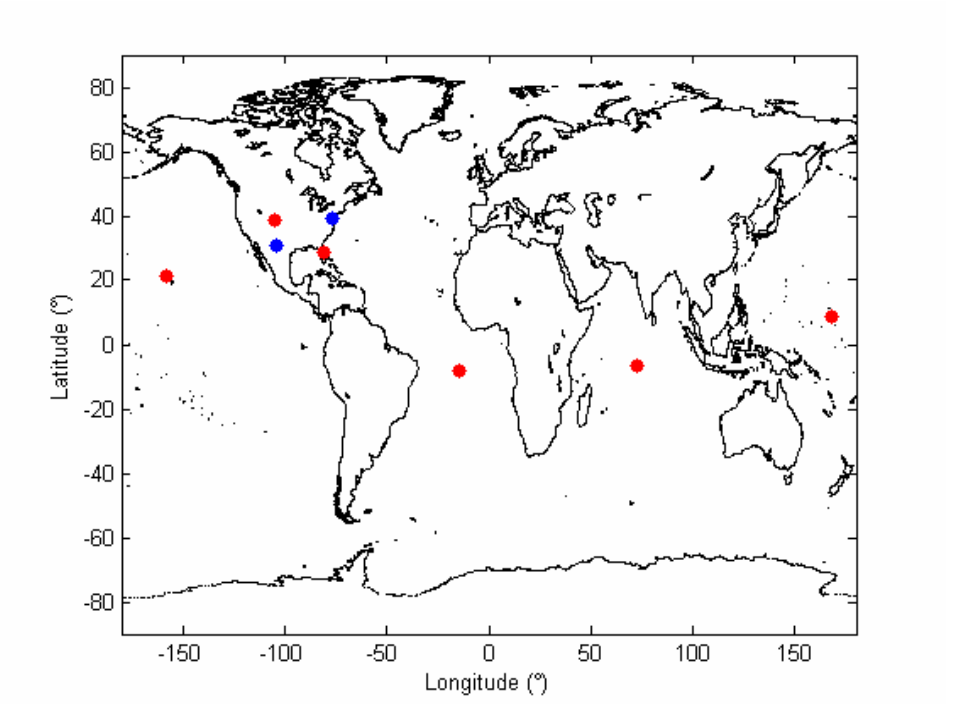

Figure 2.—MSys1 station map.

Modified System 2 (MSys2) utilizes all measurements from MSys1 plus laser ranging measurements from two additional locations. Table 4 lists the locations for the two additional ground sites used for laser ranging measurements only for MSys2. Figure 3 illustrates all of the locations of the ground sites for MSys2. The eight red dots represent stations from MSys1, while the two additional ground stations are shown in blue dots.

TABLE 4.—ADDITIONAL LASER RANGING STATION LOCATIONS— MSys2

Station	Longitude (°E)	Latitude (°N)
Hartebeesthoek	27.6861°	–27.6861°
Wuhan	114.4897°	30.5157°

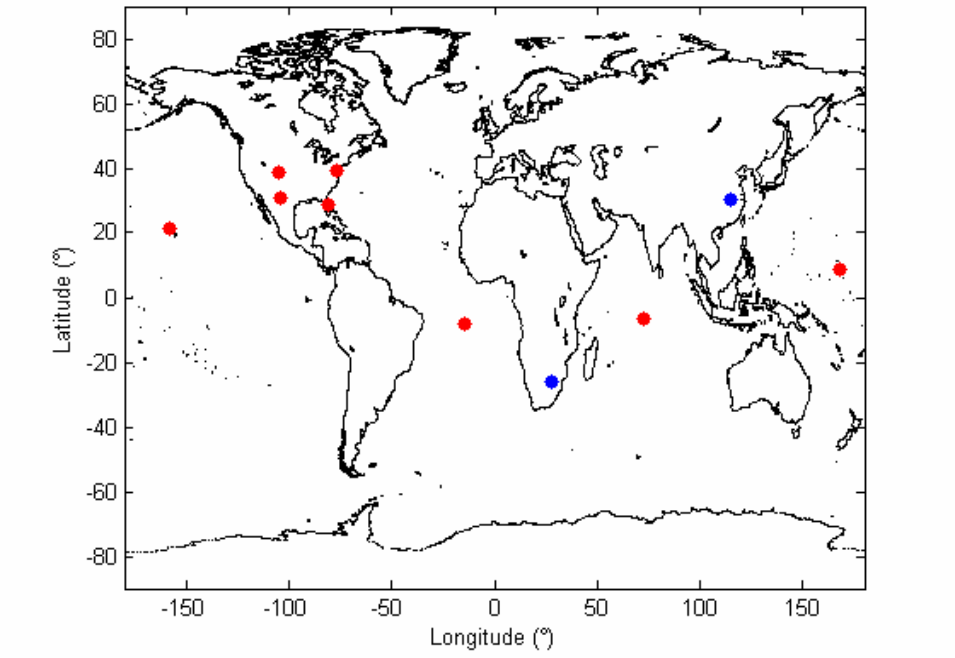

Figure 3.—MSys2 station map.

Modified System 3 (MSys3) utilizes all measurements from MSys2 plus laser ranging measurements from four additional locations. Table 5 lists the locations for the four additional ground sites used for laser ranging measurements only for MSys3. Figure 4 illustrates all of the locations of the ground sites for MSys3. The 10 red dots represent stations from MSys2, while the four additional ground stations are shown in blue dots.

TABLE 5.—ADDITIONAL LASER RANGING STATION LOCATIONS—MSys3

Station	Longitude (°E)	Latitude (°N)
Concepcion	–73.0253°	–36.8430°
Mt. Stromlo	149.0099°	–35.3161°
Komsomolsk	136.7438°	50.6946°
Metsahovi	24.3946°	60.2172°

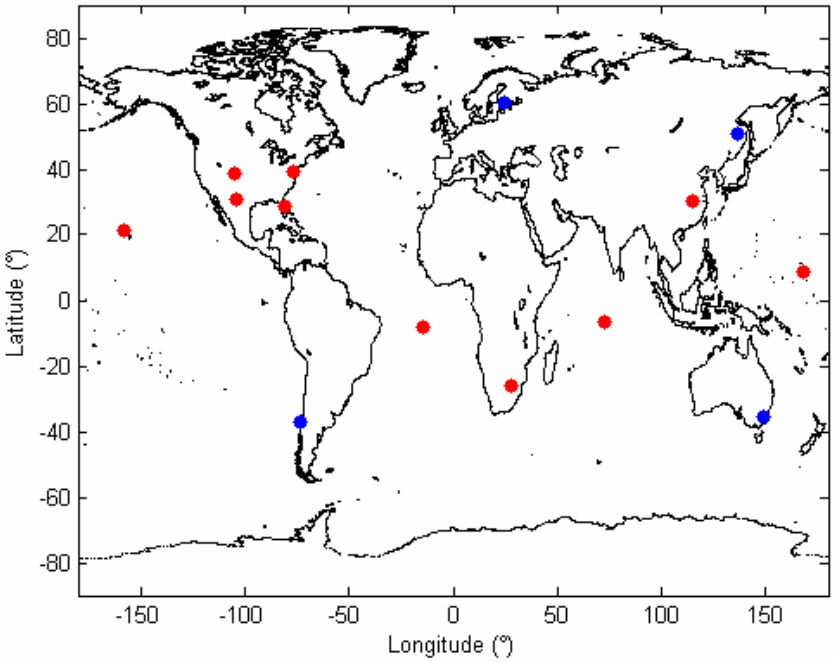

Figure 4.—MSys3 station map.

Modified System 4 (MSys4) utilizes all measurements from MSys3 plus laser ranging measurements from four additional locations. Table 6 lists the locations for the four additional ground sites used for laser ranging measurements only for MSys4. Figure 5 illustrates all of the locations of the ground sites for MSys4. The 14 red dots represent stations from MSys3, while the four additional ground stations are shown in blue dots.

TABLE 6.—ADDITIONAL LASER RANGING STATION LOCATIONS— MSys4

Station	Longitude (°E)	Latitude (°N)
Tahiti	–149.6063°	–17.5768°
Yarragadee	115.3467°	–29.0464°
San Fernando	–6.2055°	36.4650°
Urumqi	87.7100°	43.8100°

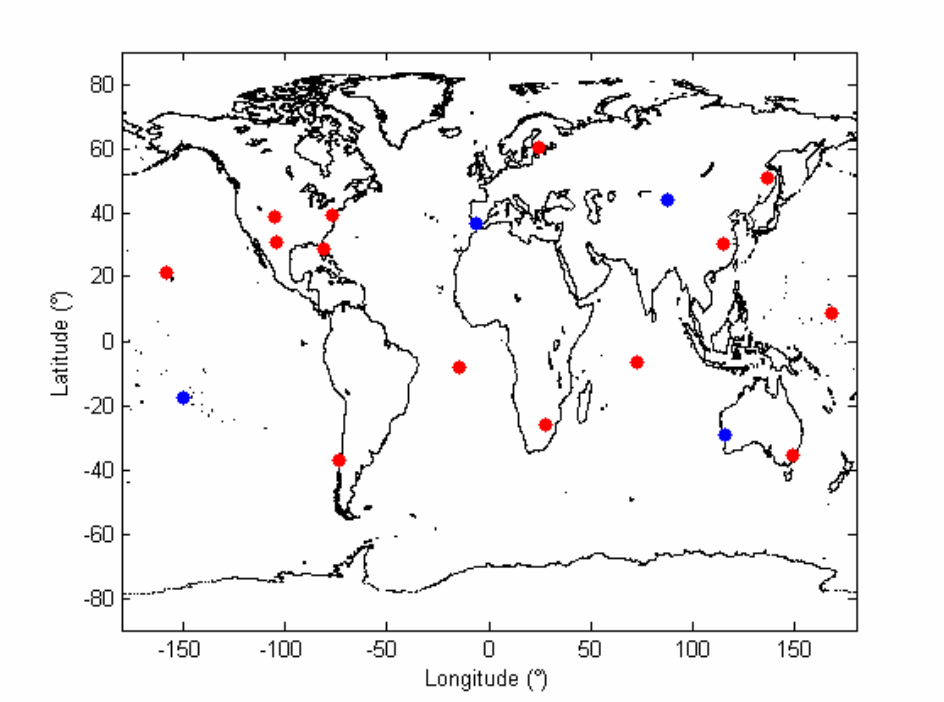

Figure 5.—MSys4 station map.

Modified System 5 (MSys5) utilizes all measurements from MSys4 plus laser ranging measurements from four additional locations. Table 7 lists the locations for the four additional ground sites used for laser ranging measurements only for MSys5. Figure 6 illustrates all of the locations of the ground sites for MSys5. The 18 red dots represent stations from MSys4, while the four additional ground stations are shown in blue dots.

TABLE 7.—ADDITIONAL LASER RANGING STATION LOCATIONS—MSys5

Station	Longitude (°E)	Latitude (°N)
Wrightwood	–117.6830°	34.3820°
Riyadh	46.4004°	24.9102°
Arequipa	–71.4930°	–16.4657°
Koganei	139.4879°	35.7102°

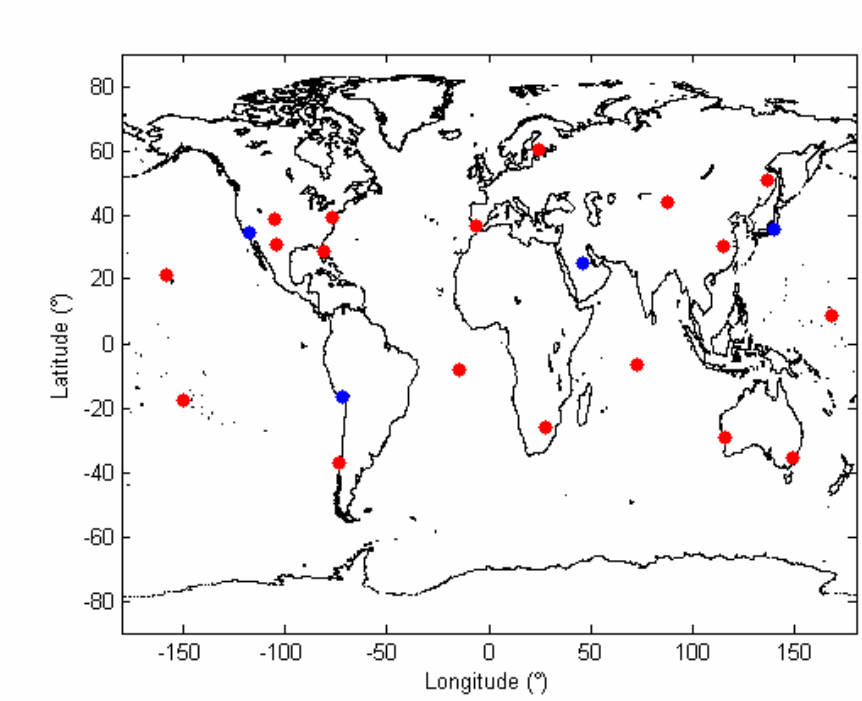

Figure 6.—Modified system 5 station map.

6. Methodology Description

The analysis is performed using the discrete time/discrete measurement EKF procedure described previously. The state is propagated at a rate of 1 Hz. The total simulation is set to run for 1 day, or 86400 seconds. It should be noted however, that measurements are not taken on this same one second time period. Pseudo-range and laser ranging measurements are taken the instant that the satellite can see the ground station, and again every 60 seconds after the initial measurement until the ground station is no longer visible.

For ADR measurements, the integration of the delta-range measurements begins the first second that the ground station is visible to the satellite. The measurement is completed once the ground station has been in view for 60 seconds. When the satellite loses visibility to the ground station, the integration procedure is reset and the satellite must start over on the next visible pass.

Note that in order for the ground station to be visible to the satellite, the ground station must see the satellite with at least a minimum elevation angle of 10°. This rule applies to all three measurement types that have been described.

The satellite is modeled in the GPS 12 hour orbit at an inclination of 55°. The orbit is assumed to start on the plane of the Earth's Equator. However, due to the nature that the ground stations are oriented on the surface, the satellite is modeled on starting longitudes of 0° and 90°E. Figures 7 and 8 show the points over the Earth surface in which the orbit for these two starting longitudes pass. Note that the point shown in red is the first point of the orbit in the simulation.

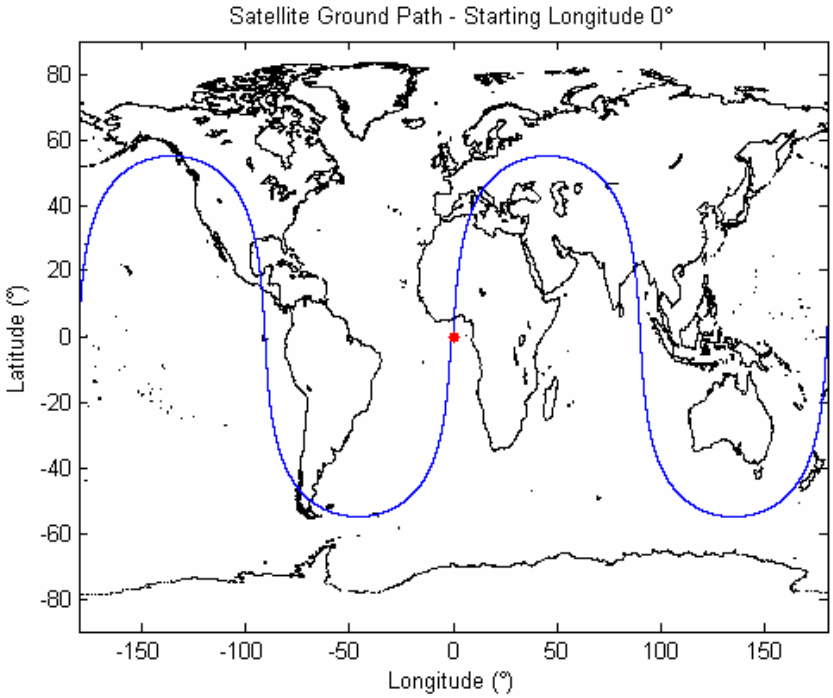

Figure 7.—Satellite ground path—starting longitude 0°.

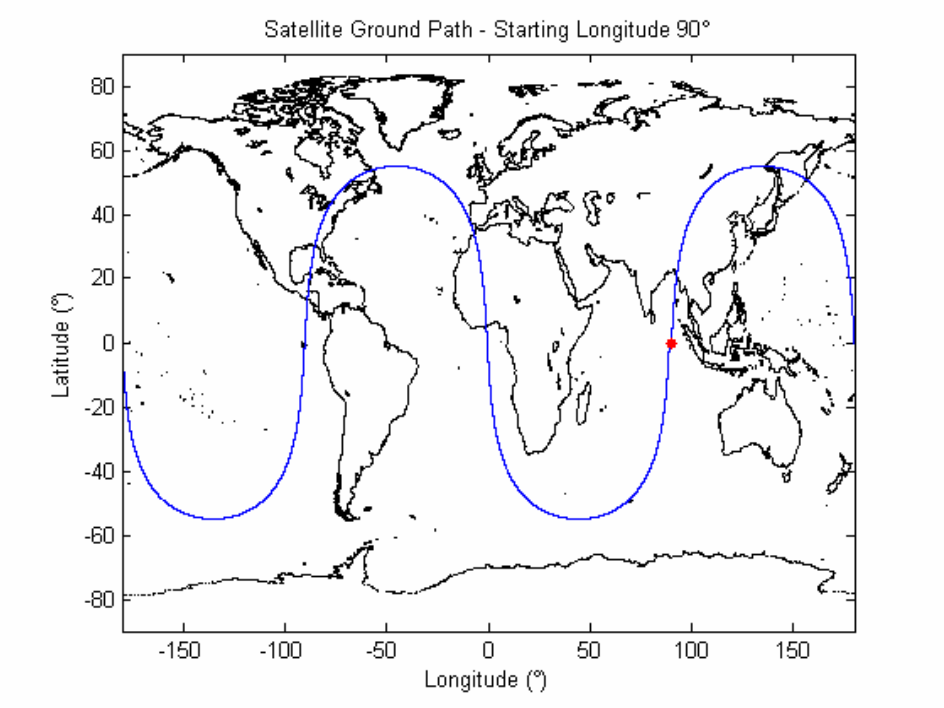

Figure 8.—Satellite ground path—starting longitude 90°.

Initial errors on the order of 1 km are added to each Cartesian dimension along with 1 m per second velocity errors in each Cartesian dimension. Clock bias and frequency bias states also begin with a 1 km and 1 m per second error, respectively. The other condition that is varied for the simulation is the initial covariance estimate. Initial conditions for the covariance estimate are formed into nine cases, as listed in table 8.

TABLE 8.—INITIAL COVARIANCE CONDITIONS

Case	Position	Velocity
1	0.1 m^2	0.1 $(m/s)^2$
2	0.1 m^2	1 $(m/s)^2$
3	0.1 m^2	10 $(m/s)^2$
4	1 m^2	0.1 $(m/s)^2$
5	1 m^2	1 $(m/s)^2$
6	1 m^2	10 $(m/s)^2$
7	10 m^2	0.1 $(m/s)^2$
8	10 m^2	1 $(m/s)^2$
9	10 m^2	10 $(m/s)^2$

Finally, for the purpose of this analysis, there will be 10 runs performed for every starting longitude/initial covariance case simulation. Performance along the multiple runs will be combined to attain overall performance.

7. Results

Results for the analysis of the comparison of the six systems are shown through the use of the covariance estimate of the systems. Even though the variance of the noise terms is constant throughout the simulations, multiple noise profiles are needed to analyze the performance of an EKF simulation. This is due to the fact that the equations of the EKF dictate that the real noise parameters, instead of the covariance of the noise, are used to form new estimates of the state. This is one difference between linear Kalman filtering and Extended Kalman Filtering. The metric to compare the performance of the six systems is range covariance, which is based on the final covariance estimate at the end of the simulation.

Equation 24 is used to compare the systems for the range covariance statistic for the covariance estimate.

$$COV_{RANGE} = \frac{1}{nlong * nrun} \sum_{i=1}^{nlong} \sum_{ii=1}^{nrun} \sqrt{P^2_{(1,1),kf,i,ii} + P^2_{(2,2),kf,i,ii} + P^2_{(3,3),kf,i,ii}} \tag{24}$$

Where:

- COV_{RANGE} is the covariance range error for the covariance estimate
- $\left(P_{(1,1),kf,i,ii}, P_{(2,2),kf,i,ii}, P_{(3,3),kf,i,ii}\right)$ are the covariance terms for the individual Cartesian dimension position terms at final time *kf* for run *ii* at longitude case *i*
- *nlong* is the number of starting longitude scenarios
- *nrun* is the number of noise profile runs

Equation (24) is used to derive performance characteristics for the six systems that are examined. Results are shown in a vertical bar graph with the system on the *x*-axis and the range covariance statistic on the *y*-axis. These bar graphs are produced a total of nine times, to account for each of the nine initial covariance cases.

Figure 9 shows the performance of the six systems under the first case of the initial covariance estimates for range covariance performance. This is when the initial covariance parameters are on the order of 0.1 m^2 and 0.1 $(m/s)^2$.

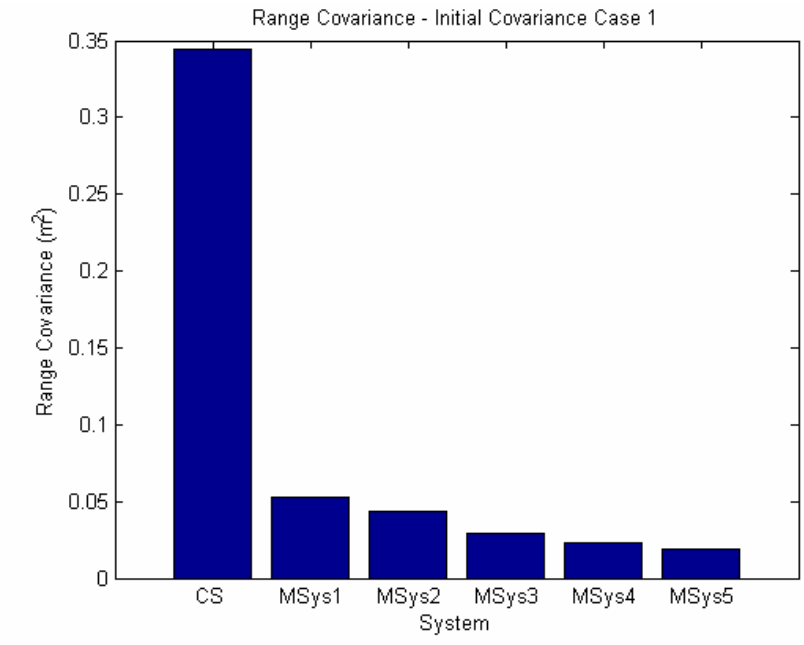

Figure 9.—Range covariance—initial covariance Case 1.

Figure 10 shows the performance of the six systems under the second case of the initial covariance estimates for range covariance performance. This is when the initial covariance parameters are on the order of 0.1 m^2 and 1 $(m/s)^2$.

Figure 11 shows the performance of the six systems under the third case of the initial covariance estimates for range covariance performance. This is when the initial covariance parameters are on the order of 0.1 m^2 and 10 $(m/s)^2$.

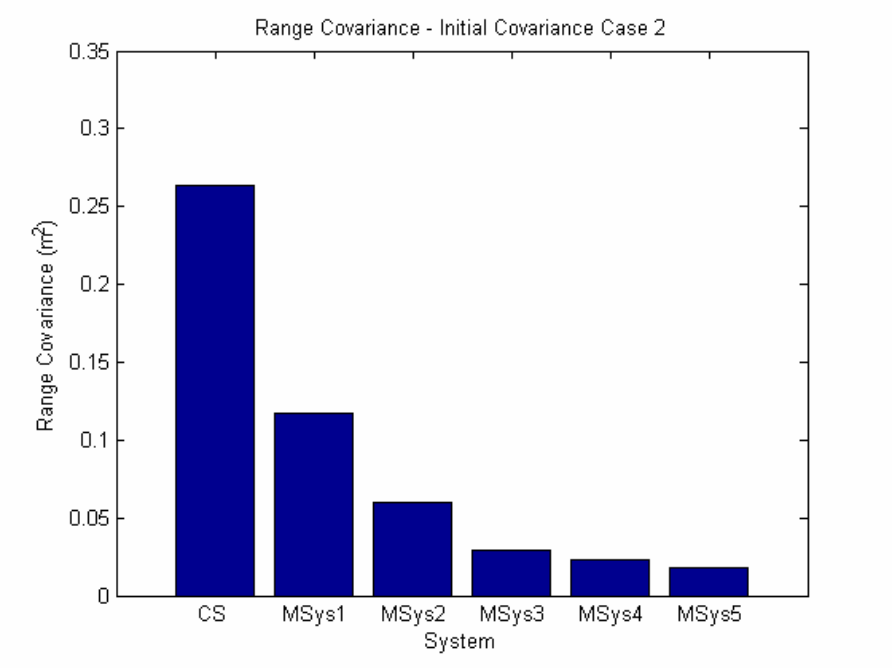

Figure 10.—Range covariance—initial covariance Case 2.

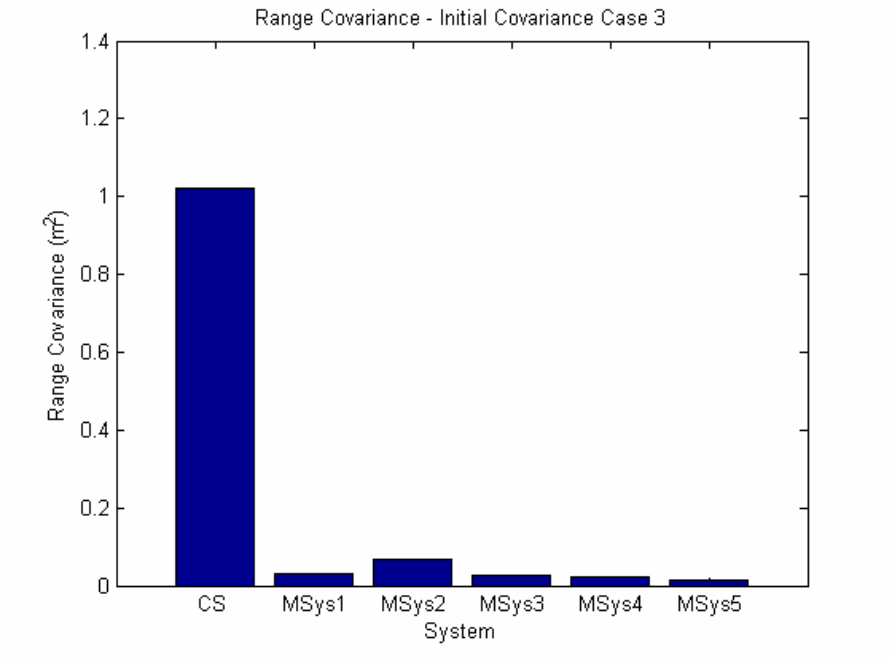

Figure 11.—Range covariance—initial covariance Case 3.

Figure 12 shows the performance of the six systems under the fourth case of the initial covariance estimates for range covariance performance. This is when the initial covariance parameters are on the order of 1 m^2 and 0.1 $(m/s)^2$.

Figure 13 shows the performance of the six systems under the fifth case of the initial covariance estimates for range covariance performance. This is when the initial covariance parameters are on the order of 1 m^2 and 1 $(m/s)^2$.

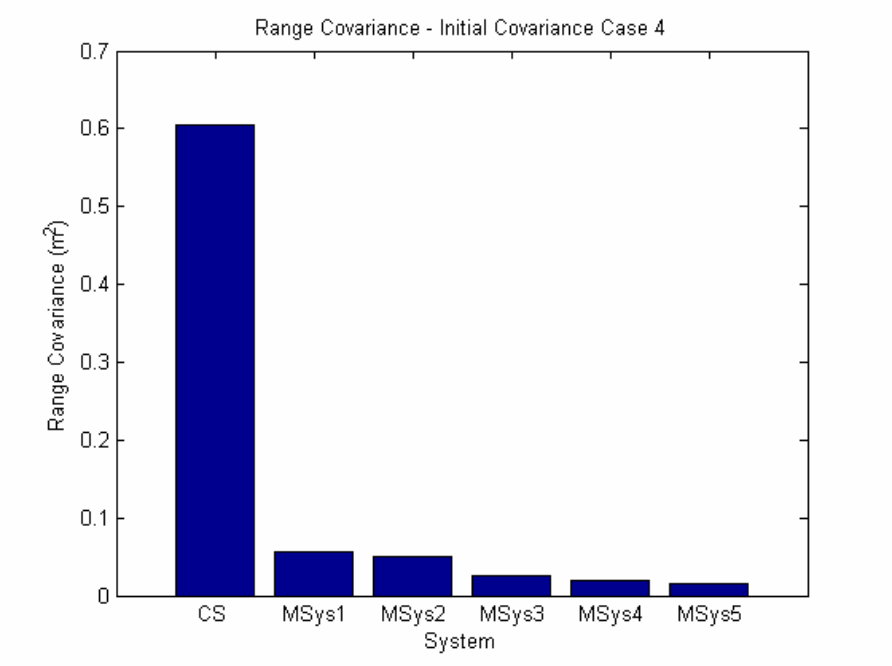

Figure 12.—Range covariance—initial covariance Case 4.

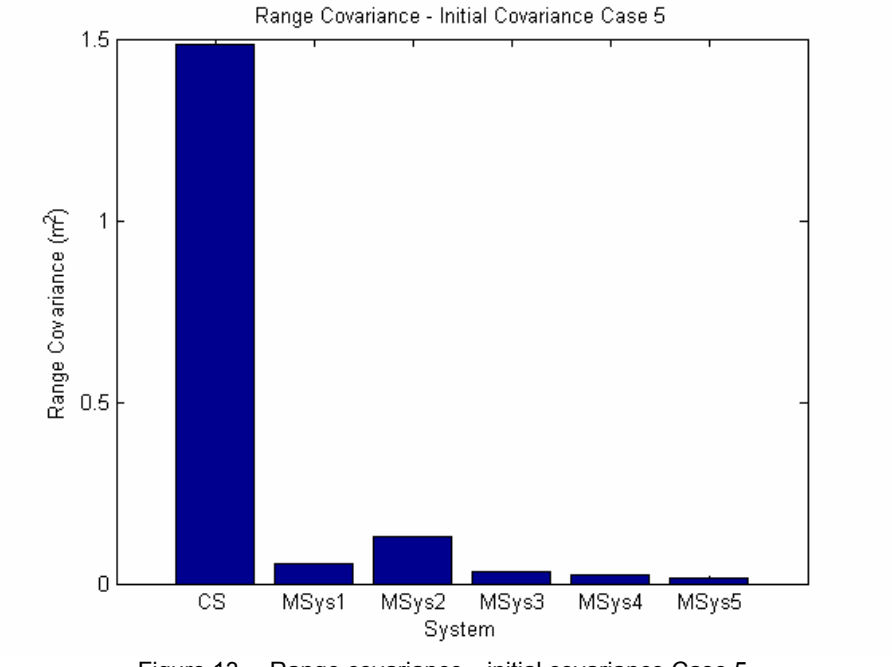

Figure 13.—Range covariance—initial covariance Case 5.

Figure 14 shows the performance of the six systems under the sixth case of the initial covariance estimates for range covariance performance. This is when the initial covariance parameters are on the order of 1 m^2 and 10 $(m/s)^2$.

Figure 15 shows the performance of the six systems under the seventh case of the initial covariance estimates for range covariance performance. This is when the initial covariance parameters are on the order of 10 m^2 and 0.1 $(m/s)^2$.

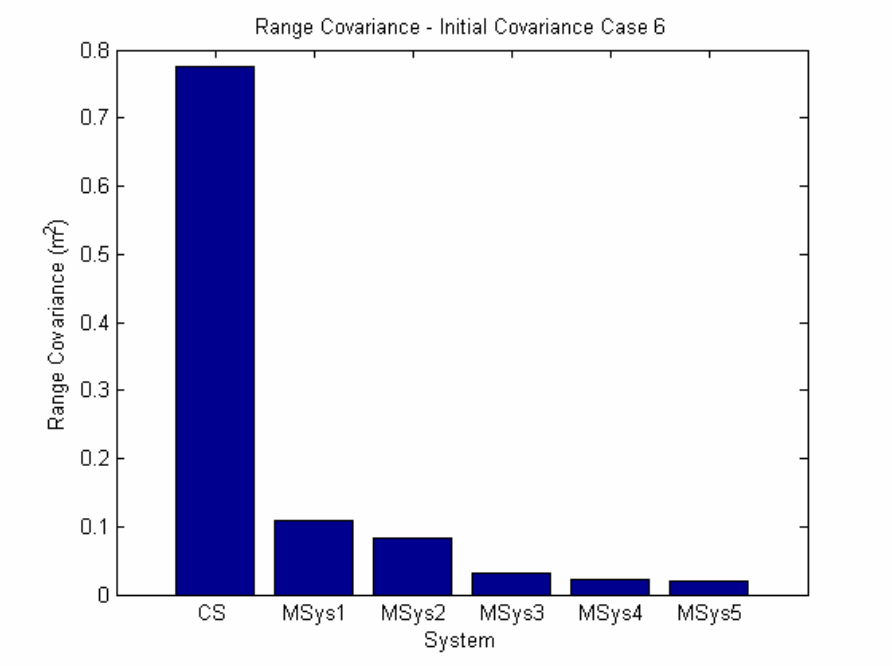

Figure 14.—Range covariance—initial covariance Case 6.

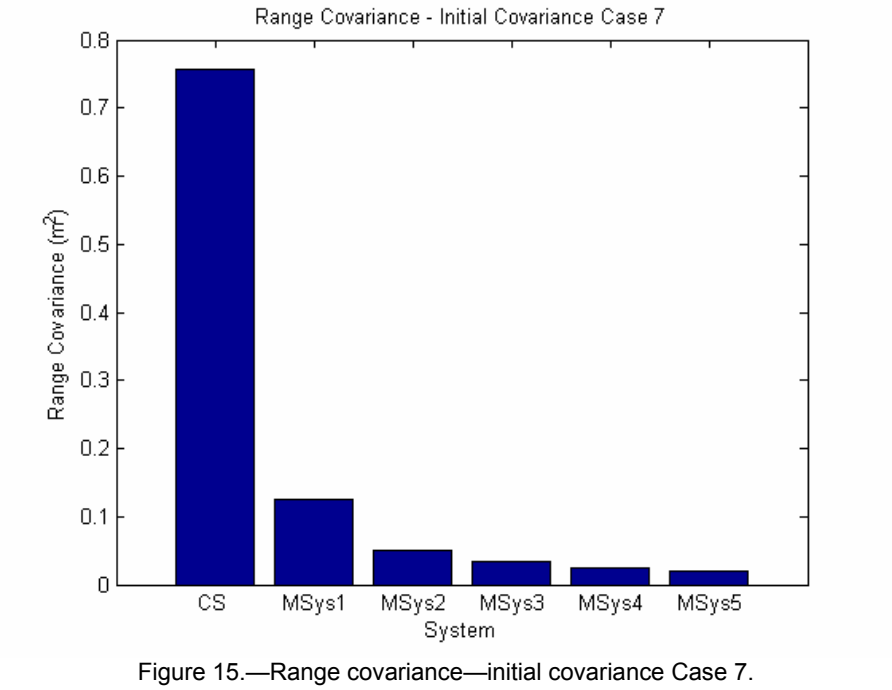

Figure 15.—Range covariance—initial covariance Case 7.

Figure 16 shows the performance of the six systems under the eighth case of the initial covariance estimates for range covariance performance. This is when the initial covariance parameters are on the order of 10 m^2 and 1 $(m/s)^2$.

Figure 17 shows the performance of the six systems under the ninth case of the initial covariance estimates for range covariance performance. This is when the initial covariance parameters are on the order of 10 m^2 and 10 $(m/s)^2$.

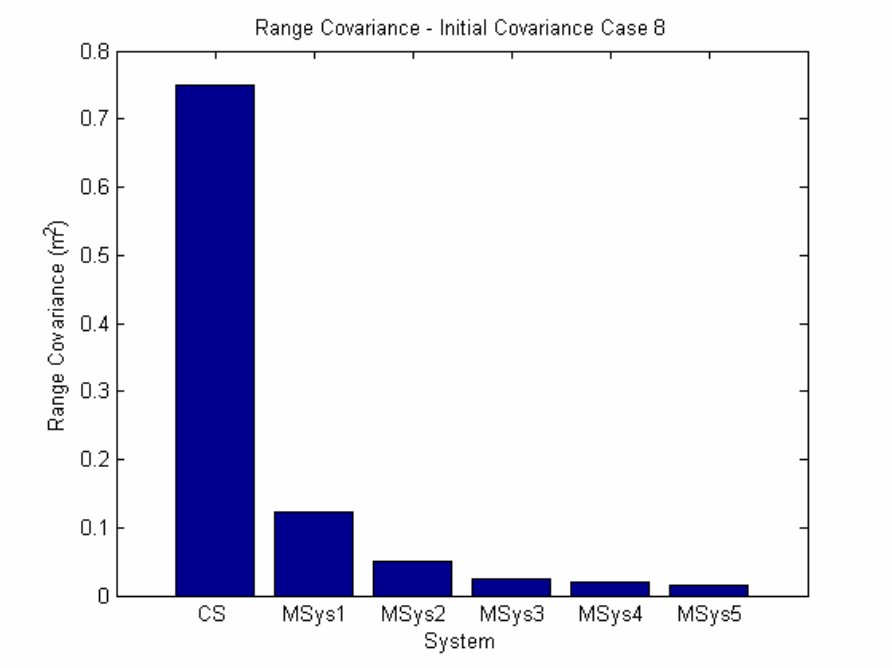

Figure 16.—Range covariance—initial covariance Case 8.

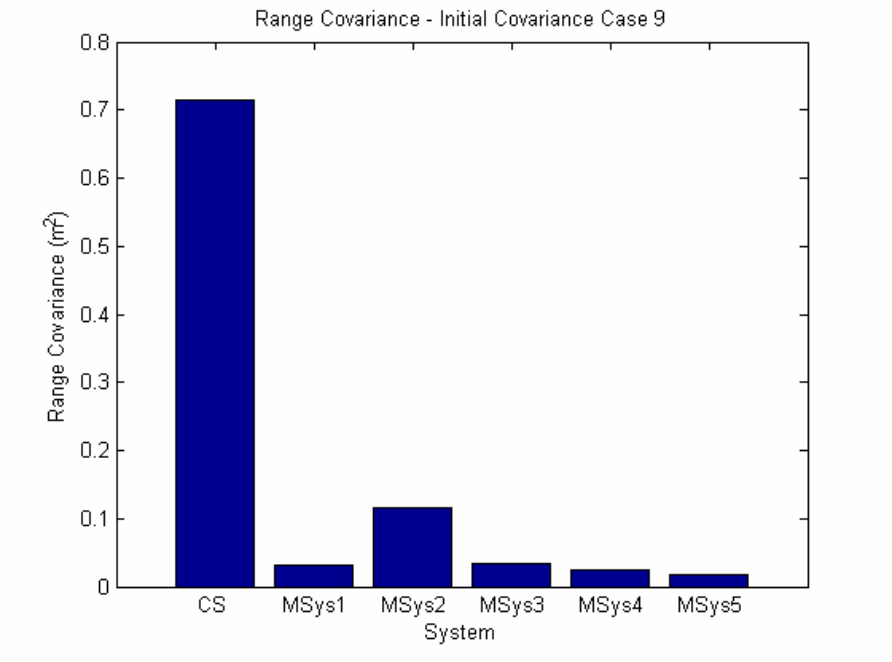

Figure 17.—Range covariance—initial covariance Case 9.

Table 9 lists the final range covariance statistics broken out by longitude versus initial covariance case. The range covariance statistics are the average of the final range covariance statistics for each run.

TABLE 9.—RANGE COVARIANCE STATISTICS BY LONGITUDE

Longitude	System	Case 1	Case 2	Case 3	Case 4	Case 5	Case 6	Case 7	Case 8	Case 9
0°	CS	0.291608	0.45046	1.510936	0.66386	2.436703	0.84973	0.883964	0.884283	1.130536
	MSys1	0.056013	0.104778	0.051748	0.065541	0.015729	0.186435	0.081631	0.198967	0.009543
	MSys2	0.03981	0.0774	0.122318	0.044429	0.24755	0.115746	0.045028	0.045007	0.172855
	MSys3	0.030392	0.030389	0.030389	0.03339	0.033389	0.033389	0.033764	0.033764	0.033764
	MSys4	0.02429	0.024288	0.024288	0.025982	0.025981	0.025979	0.026182	0.026181	0.02618
	MSys5	0.019915	0.019914	0.019878	0.020988	0.020987	0.020985	0.02111	0.02111	0.021109
90°E	CS	0.398027	0.076659	0.534994	0.545768	0.530322	0.69956	0.628294	0.61492	0.298915
	MSys1	0.049903	0.129587	0.009439	0.048682	0.090065	0.030502	0.169729	0.044325	0.054874
	MSys2	0.046169	0.041485	0.012127	0.055961	0.012876	0.05139	0.057204	0.057459	0.056998
	MSys3	0.028958	0.028939	0.026205	0.015941	0.030104	0.031659	0.031912	0.015938	0.032032
	MSys4	0.022156	0.021378	0.019173	0.01187	0.021379	0.019558	0.023869	0.01186	0.02387
	MSys5	0.017915	0.016662	0.011083	0.011044	0.013626	0.016653	0.018862	0.010178	0.012779

Profiles for the range covariance parameters are shown in Appendix A. It is important to notice how the starting longitude and initial starting covariance affect the performance for each of the systems. It is easy to visualize from the graphics that the initial covariance cases in which the velocity terms have a lower/equal initial covariance than the position terms perform more consistently, compared to when the velocity terms have larger initial covariance terms than the position terms.

It should also be noted at this time about an issue that arose during the simulations. Other starting longitudes of 180°E and 90°W were run, but there was difficulty with the numerical stability of the simulations. The difficulty was repeatability of the simulation results on different computers. Duplications of the simulations were run on various computers with common noise profiles and other parameters, with differing results. Issues that were seen included non-symmetric covariance matrices and differences in the inversions of ill-conditioned matrices. Possible resolution of this issue will be discussed in the Future Work section.

8. Conclusions

Results for the comparison between the current tracking system utilizing pseudo-range and ADR measurements from the six MS locations with the five modified systems including laser ranging measurements from the same ground sites plus additional sites have been provided. All of the results show benefits of having laser ranging measurements used to solve for the satellite's position component of the state vector. The results show an initial dependency on the initial longitude of the orbit. A second parameter that has been shown to affect performance is the initial covariance for the system. However, for both of these parameters, the final covariance is not strongly affected.

The parameter that does strongly affect the final time covariance is the number of laser ranging ground stations used. As seen in the results in figures 9 through 17, it is typical that with an increase in the number of laser ranging ground stations, the final time range covariance statistic decreases. It is important to note that as more and more ground stations are added to the scenario, that the final time covariance does not keep decreasing more and more. This means that after a certain point, there exists a value of the number of laser ranging ground stations for which there is little decrease in the final time range covariance. The plots that are provided in Appendix A illustrate this effect, even when the y-axis is plotted in log scale.

The initial covariance of the state is an estimate for how well the state is understood. Typically, when the state's covariance is larger, then more emphasis is placed on the measurements when producing the EKF Kalman gain. However, when dealing with an OD type of analysis similar to the one performed,

where and when there are few measurements available to the receiver, then covariance parameters can increase tremendously. Also, the covariance of the measurement noise is an important parameter for how the covariance is propagated.

Therefore, in order to better estimate the performance of the system, there needs to be more tracking measurements available to be used in the EKF, especially in the beginning time periods of the simulation. This can be provided in two forms. First, there can be more tracking sites used to provide measurements. Second, measurements can be taken more frequently. Modifying these options was not analyzed in this initial study. The first option would mean removing ground stations at some point in time in the simulation, where this simulation assumed that the ground station would be present throughout the entirety of the simulation. Also, variations in measurement noise covariance were not considered for this study.

Results shown from this study include the fact that there are differences in performance between the current system and the modified systems including laser ranging measurements. Performance is dependent on the location of the ground stations and how those stations are viewed by the satellite. Therefore, if the additional ground stations for the modified systems were picked differently, then the results would vary. Therefore, elevation angle that is seen from the ground to the satellite affects performance. It is believed that if constraints (such as range and/or speed) are placed within the EKF, performance of the two systems may be better modeled.

The question that needs to be answered from the analysis is if laser ranging measurements are needed, and if so, then how many stations are necessary. First off, the answer depends on the requirements. In stating this, it is acknowledged that the requirements will state a certain covariance level needed. This should be the ultimate answer as to what system to use. However, this analysis has shown that laser ranging measurements are beneficial and reduce the steady state system performance. Typically, the more stations that are added to the scenario, the lower the steady state system performance will be. However, there is little change in system performance when going from MSys3 to MSys4 and then from MSys4 to MSys5. Therefore, given the orientation of the ground stations as such as in this report, it appears that MSys3 would give the most benefit. Therefore, it is believed that if laser ranging measurements would in the future be taken into account for doing OD analysis on a GPS orbit, then the recommendation would be have measurements taken from the six MS stations with measurements from an additional eight ground stations around the world.

9. Future Work

Future work in the area of OD determination for a GPS orbit comparing the current system of pseudo-range and ADR measurements with modified systems using varying numbers of laser ranging ground stations, pseudo-range and ADR measurements can be expanded in multiple methods. The following list is not a complete list on what can be performed to enhance the analysis provided here, but is what the author believes to be an important next step.

- Model scenario with a form of square root/U-D filtering to improve numerical stability issues that arise from using finite numerical processing
- Model scenario with a 2nd order EKF
- Perform parametric analysis with variations in how often measurements are taken
- Perform parametric analysis with variations in measurement covariance
- Perform further parametric analysis on starting latitude and longitude
- Perform smoothing on all past state estimates for the purpose of obtaining a better estimate of new state estimates
- Perform smoothing on all state estimates for the purpose of obtaining a better estimate all state estimates
- Include orbital perturbations to make scenario more realistic

Appendix A—Range Covariance Results

A.1. Initial Covariance Case 1 Results

Figures A.1.1 and A.1.2 show the range covariance results for the 0° and 90°E starting longitude conditions, respectively, when the initial covariance is operating in Case 1 parameters (Cartesian position components = 0.1 m^2, Cartesian velocity components = 0.1 $(m/s)^2$). Blue lines represent range covariance results for the current system based on pseudo-range and ADR measurements from the 6 MS ground stations. Red lines represent range covariance results for MSys1, combining the current system with laser ranging measurements from the 6 MS stations and 2 additional ground stations. Similarly, black lines represent range covariance results for MSys2; green lines represent range covariance results for MSys3; cyan lines represent range covariance results for MSys4; yellow lines represent range covariance results for MSys5. Note that there are 10 individual lines for each color, derived from the 10 noise profile runs.

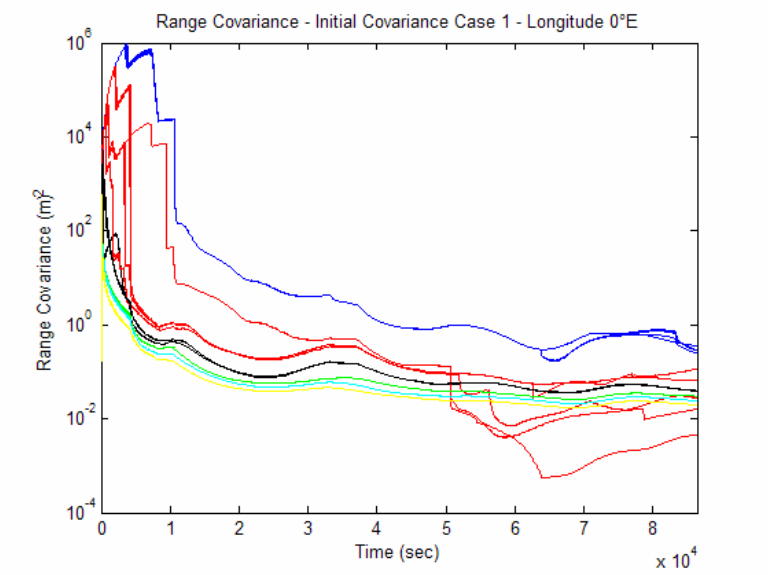

Figure A.1.1.—Starting longitude 0° results.

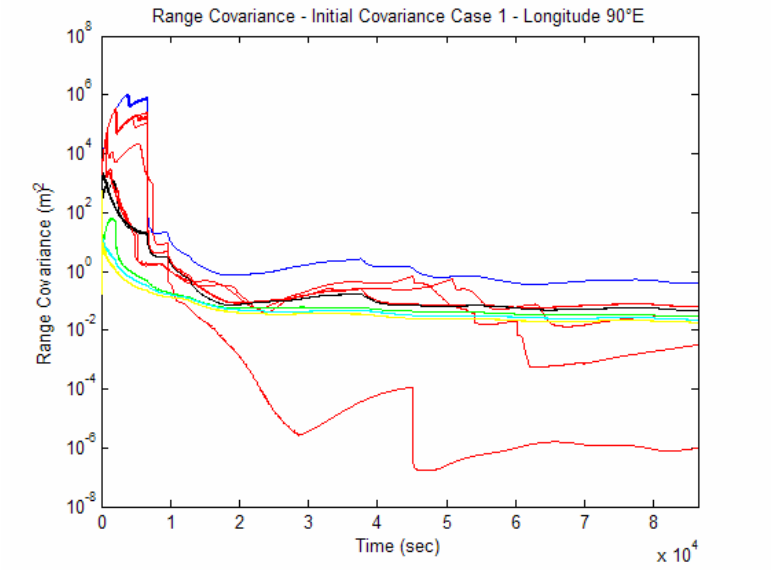

Figure A.1.2.—Starting longitude 90° results.

A.2. Initial Covariance Case 2 Results

Figures A.2.1 and A.2.2 show the range covariance results for the 0° and 90°E starting longitude conditions, respectively, when the initial covariance is operating in Case 2 parameters (Cartesian position components = 0.1 m^2, Cartesian velocity components = 1 $(m/s)^2$). Blue lines represent range covariance results for the current system based on pseudo-range and ADR measurements from the 6 MS ground stations. Red lines represent range covariance results for MSys1, combining the current system with laser ranging measurements from the 6 MS stations and 2 additional ground stations. Similarly, black lines represent range covariance results for MSys2; green lines represent range covariance results for MSys3; cyan lines represent range covariance results for MSys4; yellow lines represent range covariance results for MSys5. Note that there are 10 individual lines for each color, derived from the 10 noise profile runs.

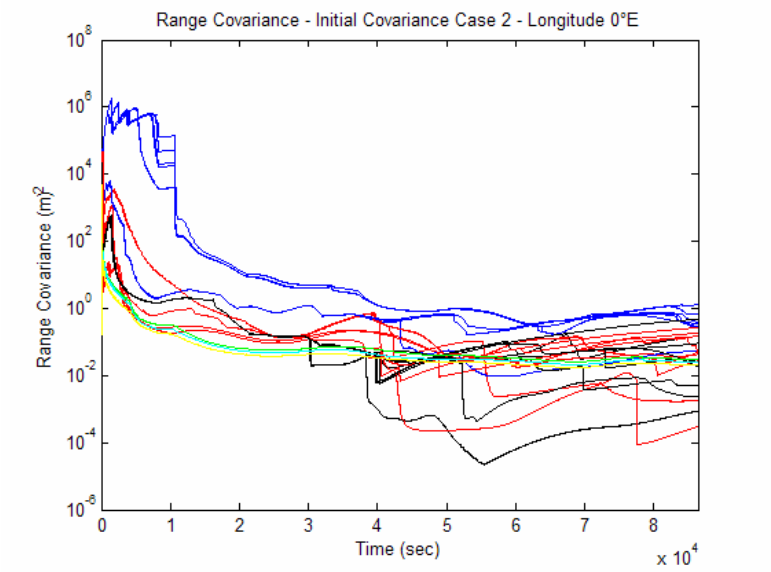

Figure A.2.1.—Starting longitude 0° results.

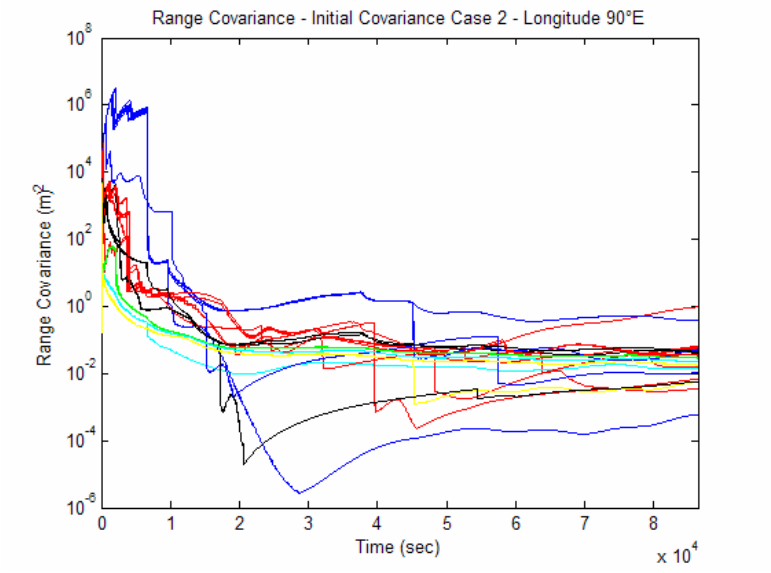

Figure A.2.2.—Starting longitude 90° results.

A.3. Initial Covariance Case 3 Results

Figures A.3.1 and A.3.2 show the range covariance results for the 0° and 90°E starting longitude conditions, respectively, when the initial covariance is operating in Case 3 parameters (Cartesian position components = 0.1 m^2, Cartesian velocity components = 10 $(m/s)^2$). Blue lines represent range covariance results for the current system based on pseudo-range and ADR measurements from the 6 MS ground stations. Red lines represent range covariance results for MSys1, combining the current system with laser ranging measurements from the 6 MS stations and 2 additional ground stations. Similarly, black lines represent range covariance results for MSys2; green lines represent range covariance results for MSys3; cyan lines represent range covariance results for MSys4; yellow lines represent range covariance results for MSys5. Note that there are 10 individual lines for each color, derived from the 10 noise profile runs.

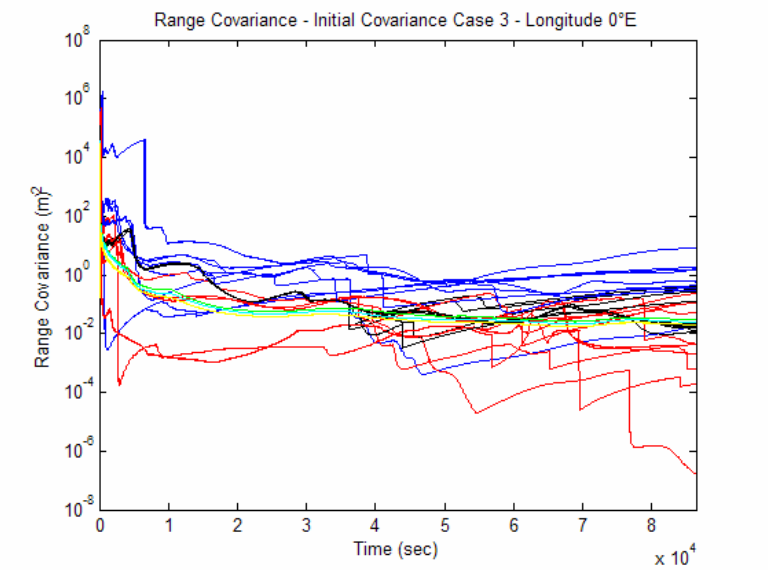

Figure A.3.1.—Starting longitude 0° results.

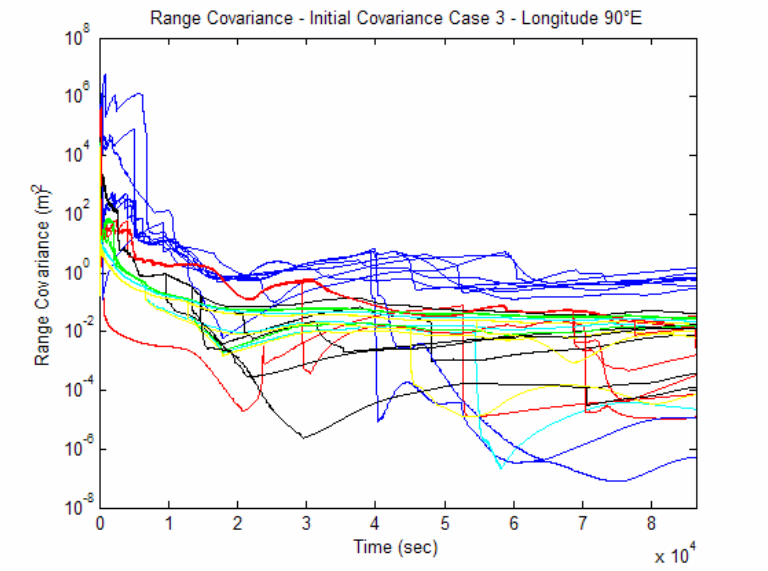

Figure A.3.2.—Starting longitude 90° results.

A.4. Initial Covariance Case 4 Results

Figures A.4.1 and A.4.2 show the range covariance results for the 0° and 90°E starting longitude conditions, respectively, when the initial covariance is operating in Case 4 parameters (Cartesian position components = 1 m^2, Cartesian velocity components = 0.1 $(m/s)^2$). Blue lines represent range covariance results for the current system based on pseudo-range and ADR measurements from the 6 MS ground stations. Red lines represent range covariance results for MSys1, combining the current system with laser ranging measurements from the 6 MS stations and 2 additional ground stations. Similarly, black lines represent range covariance results for MSys2; green lines represent range covariance results for MSys3; cyan lines represent range covariance results for MSys4; yellow lines represent range covariance results for MSys5. Note that there are 10 individual lines for each color, derived from the 10 noise profile runs.

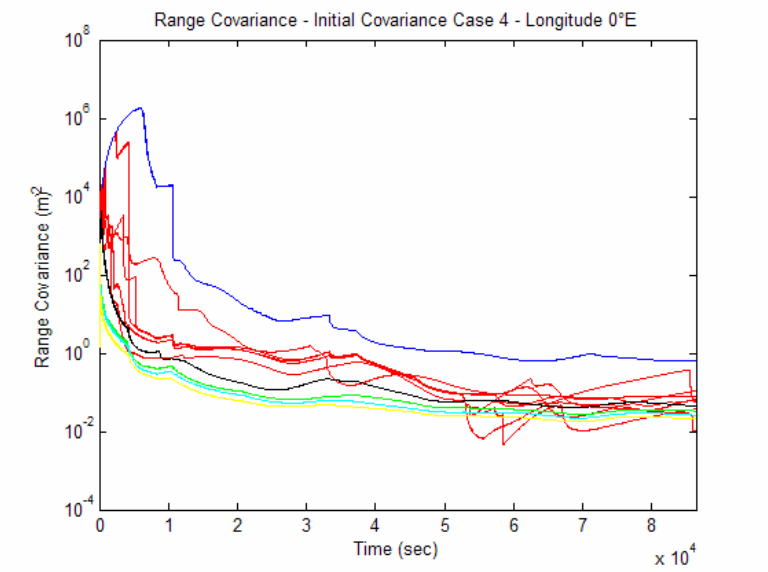

Figure A.4.1.—Starting longitude 0° results.

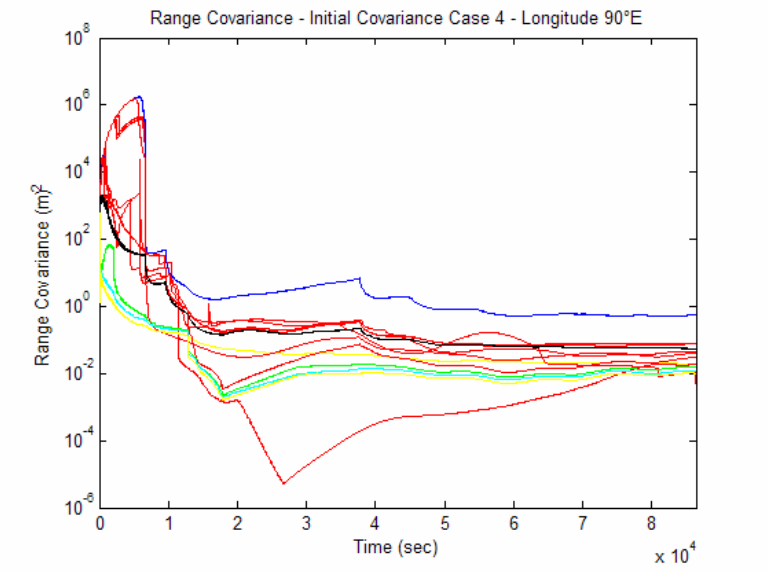

Figure A.4.2.—Starting longitude 90° results.

A.5. Initial Covariance Case 5 Results

Figures A.5.1 and A.5.2 show the range covariance results for the 0° and 90°E starting longitude conditions, respectively, when the initial covariance is operating in Case 5 parameters (Cartesian position components = 1 m^2, Cartesian velocity components = 1 $(m/s)^2$). Blue lines represent range covariance results for the current system based on pseudo-range and ADR measurements from the 6 MS ground stations. Red lines represent range covariance results for MSys1, combining the current system with laser ranging measurements from the 6 MS stations and 2 additional ground stations. Similarly, black lines represent range covariance results for MSys2; green lines represent range covariance results for MSys3; cyan lines represent range covariance results for MSys4; yellow lines represent range covariance results for MSys5. Note that there are 10 individual lines for each color, derived from the 10 noise profile runs.

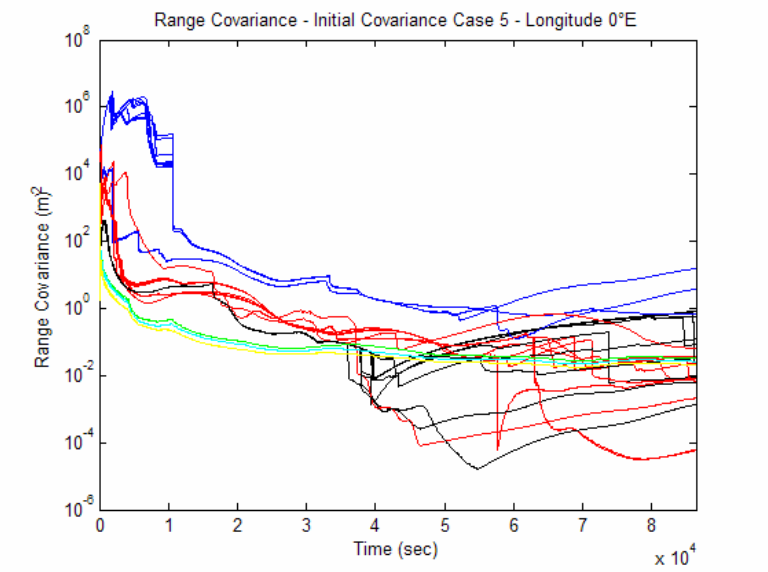

Figure A.5.1.—Starting longitude 0° results.

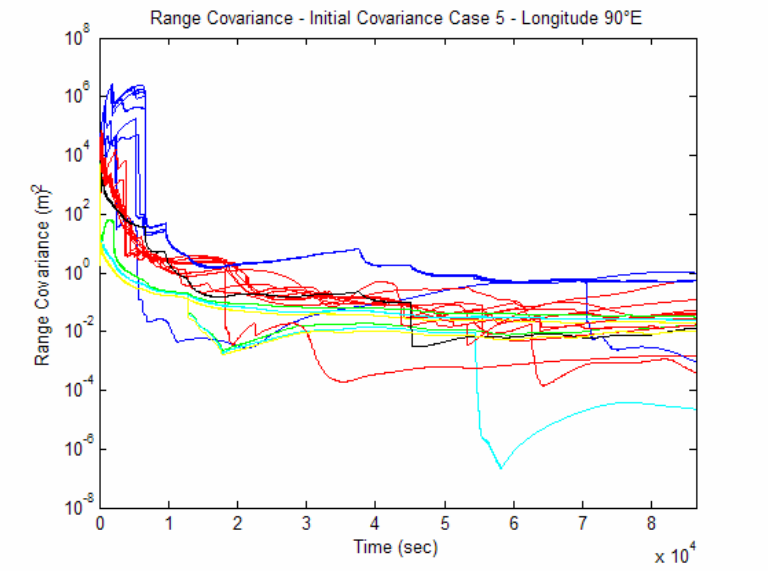

Figure A.5.2.—Starting longitude 90° results.

A.6. Initial Covariance Case 6 Results

Figures A.6.1 and A.6.2 show the range covariance results for the 0° and 90°E starting longitude conditions, respectively, when the initial covariance is operating in Case 6 parameters (Cartesian position components = 1 m^2, Cartesian velocity components = 10 $(m/s)^2$). Blue lines represent range covariance results for the current system based on pseudo-range and ADR measurements from the 6 MS ground stations. Red lines represent range covariance results for MSys1, combining the current system with laser ranging measurements from the 6 MS stations and 2 additional ground stations. Similarly, black lines represent range covariance results for MSys2; green lines represent range covariance results for MSys3; cyan lines represent range covariance results for MSys4; yellow lines represent range covariance results for MSys5. Note that there are 10 individual lines for each color, derived from the 10 noise profile runs.

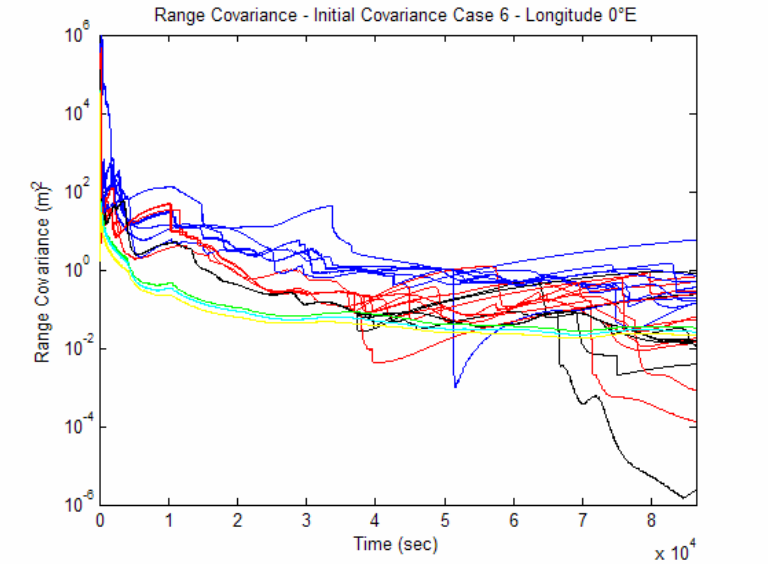

Figure A.6.1.—Starting longitude 0° results.

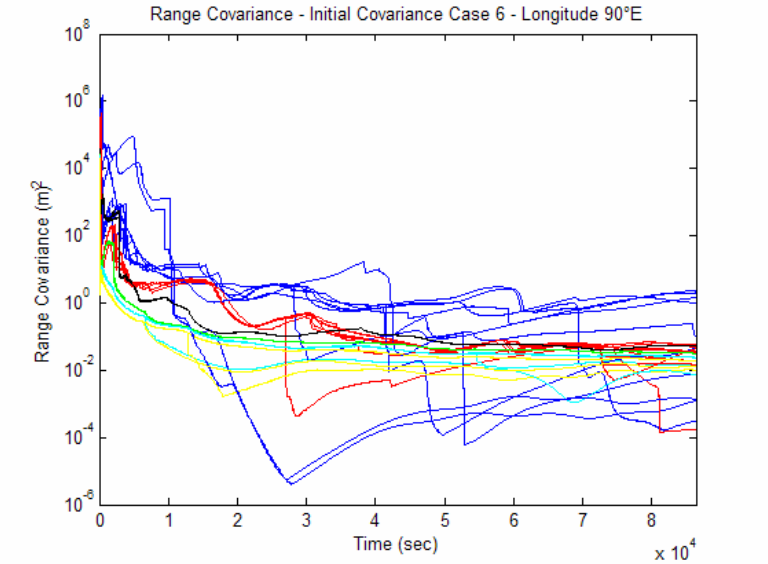

Figure A.6.2.—Starting longitude 90° results.

A.7. Initial Covariance Case 7 Results

Figures A.7.1 and A.7.2 show the range covariance results for the 0° and 90°E starting longitude conditions, respectively, when the initial covariance is operating in Case 7 parameters (Cartesian position components = 10 m^2, Cartesian velocity components = 0.1 $(m/s)^2$). Blue lines represent range covariance results for the current system based on pseudo-range and ADR measurements from the 6 MS ground stations. Red lines represent range covariance results for MSys1, combining the current system with laser ranging measurements from the 6 MS stations and 2 additional ground stations. Similarly, black lines represent range covariance results for MSys2; green lines represent range covariance results for MSys3; cyan lines represent range covariance results for MSys4; yellow lines represent range covariance results for MSys5. Note that there are 10 individual lines for each color, derived from the 10 noise profile runs.

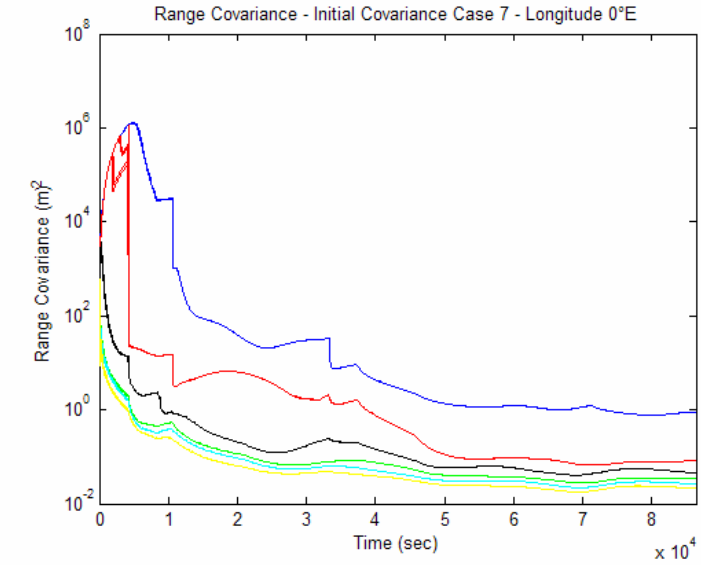

Figure A.7.1.—Starting longitude 0° results.

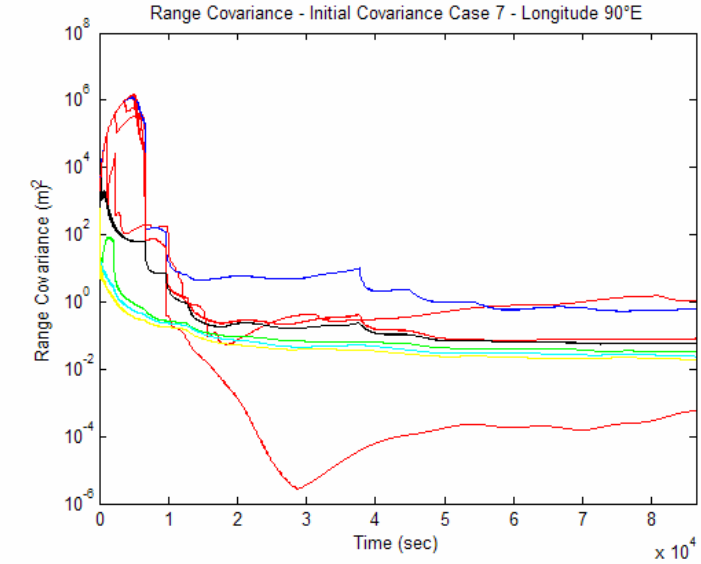

Figure A.7.2.—Starting longitude 90° results.

A.8. Initial Covariance Case 8 Results

Figures A.8.1 and A.8.2 show the range covariance results for the 0° and 90°E starting longitude conditions, respectively, when the initial covariance is operating in Case 8 parameters (Cartesian position components = 10 m^2, Cartesian velocity components = 1 $(m/s)^2$). Blue lines represent range covariance results for the current system based on pseudo-range and ADR measurements from the 6 MS ground stations. Red lines represent range covariance results for MSys1, combining the current system with laser ranging measurements from the 6 MS stations and 2 additional ground stations. Similarly, black lines represent range covariance results for MSys2; green lines represent range covariance results for MSys3; cyan lines represent range covariance results for MSys4; yellow lines represent range covariance results for MSys5. Note that there are 10 individual lines for each color, derived from the 10 noise profile runs.

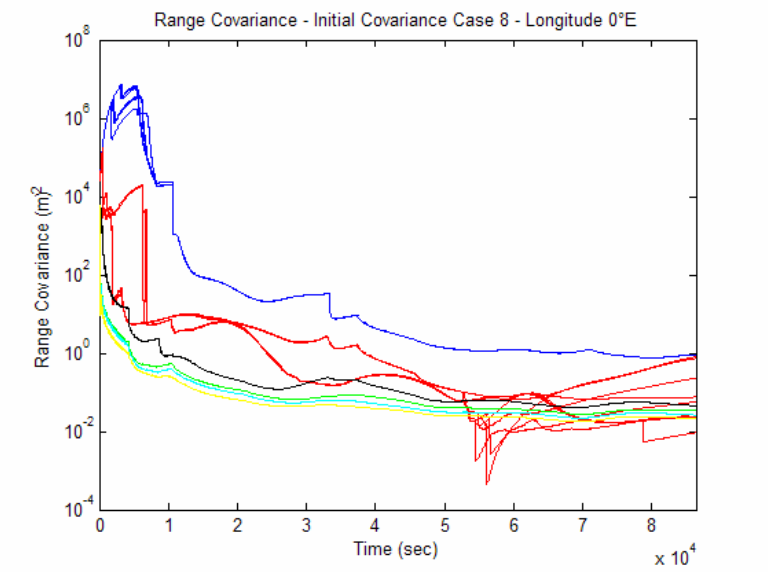

Figure A.8.1.—Starting longitude 0° results.

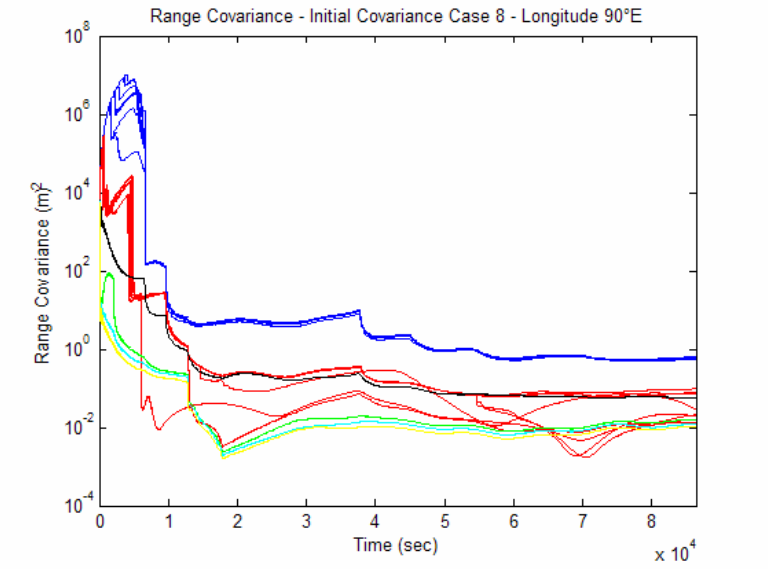

Figure A.8.2.—Starting longitude 90° results.

A.9. Initial Covariance Case 9 Results

Figures A.9.1 and A.9.2 show the range covariance results for the 0° and 90°E starting longitude conditions, respectively, when the initial covariance is operating in Case 9 parameters (Cartesian position components = 10 m^2, Cartesian velocity components = 10 $(m/s)^2$). Blue lines represent range covariance results for the current system based on pseudo-range and ADR measurements from the 6 MS ground stations. Red lines represent range covariance results for MSys1, combining the current system with laser ranging measurements from the 6 MS stations and 2 additional ground stations. Similarly, black lines represent range covariance results for MSys2; green lines represent range covariance results for MSys3; cyan lines represent range covariance results for MSys4; yellow lines represent range covariance results for MSys5. Note that there are 10 individual lines for each color, derived from the 10 noise profile runs.

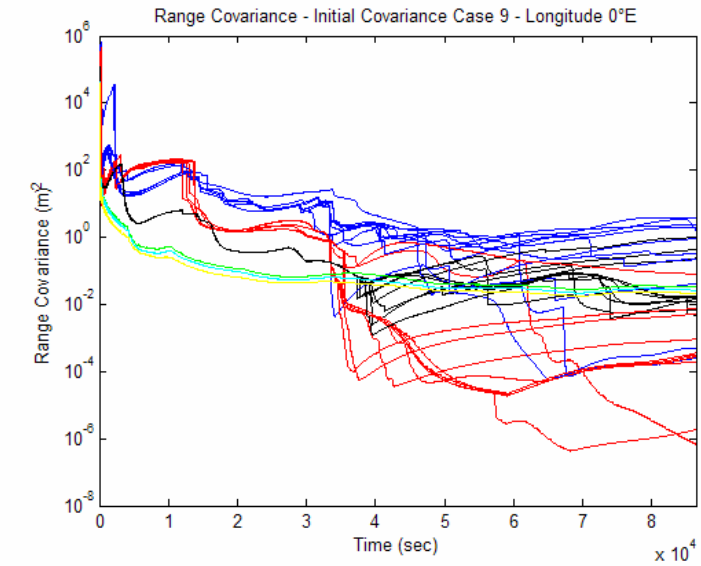

Figure A.9.1.—Starting longitude 0° results.

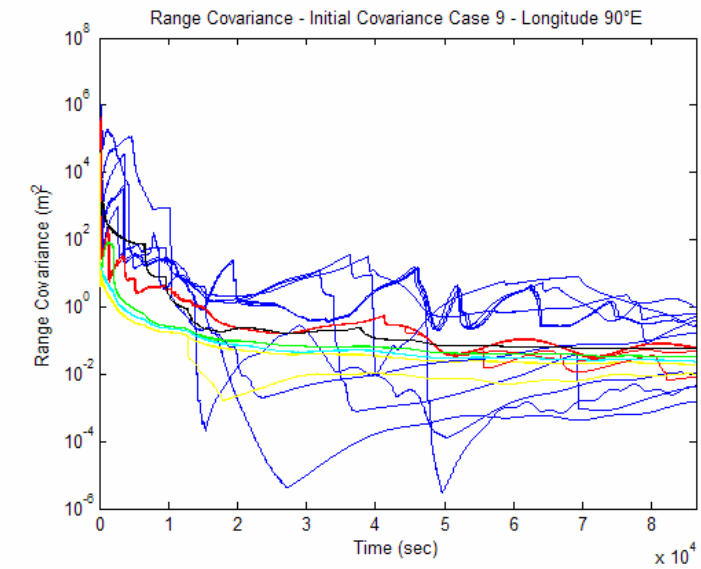

Figure A.9.2.—Starting longitude 90° results.

References

1. Dan Simon, Optimal State Estimation, John Wiley & Sons, 2006.
2. James R Wertz and Wiley J. Larson, Space Mission Analysis and Design, Microcosm Press, 1999.
3. Mohinder S. Grewal, Lawrence R. Weill, & Angus P. Andrews, Global Positioning Systems, Inertial Navigation and Integration, John Wiley & Sons, 2001.
4. International Laser Ranging Service, http://ilrs.gsfc.nasa.gov/, August 2006.

REPORT DOCUMENTATION PAGE

Form Approved
OMB No. 0704-0188

1. AGENCY USE ONLY (*Leave blank*)	2. REPORT DATE	3. REPORT TYPE AND DATES COVERED
	February 2007	Technical Memorandum

4. TITLE AND SUBTITLE

Orbit Determination Analysis Utilizing Radiometric and Laser Ranging Measurements for GPS Orbit

5. FUNDING NUMBERS

WBS 439432.07.04.03.01

6. AUTHOR(S)

Bryan W. Welch

7. PERFORMING ORGANIZATION NAME(S) AND ADDRESS(ES)

National Aeronautics and Space Administration
John H. Glenn Research Center at Lewis Field
Cleveland, Ohio 44135–3191

8. PERFORMING ORGANIZATION REPORT NUMBER

E–15815

9. SPONSORING/MONITORING AGENCY NAME(S) AND ADDRESS(ES)

National Aeronautics and Space Administration
Washington, DC 20546–0001

10. SPONSORING/MONITORING AGENCY REPORT NUMBER

NASA TM—2007-214679

11. SUPPLEMENTARY NOTES

Responsible person, Bryan W. Welch, organization code RCI, 216–433–3390.

12a. DISTRIBUTION/AVAILABILITY STATEMENT

Unclassified - Unlimited
Subject Category: 17

Available electronically at http://gltrs.grc.nasa.gov

This publication is available from the NASA Center for AeroSpace Information, 301–621–0390.

12b. DISTRIBUTION CODE

13. ABSTRACT ***(Maximum 200 words)***

While navigation systems for the determination of the orbit of the Global Position System (GPS) have proven to be very effective, the current issues involve lowering the error in the GPS satellite ephemerides below their current level. In this document, the results of an orbit determination covariance assessment are provided. The analysis is intended to be the baseline orbit determination study comparing the benefits of adding laser ranging measurements from various numbers of ground stations. Results are shown for two starting longitude assumptions of the satellite location and for nine initial covariance cases for the GPS satellite state vector.

14. SUBJECT TERMS

Global positioning system; Navigation; Space navigation; Positioning; Orbit determination; State estimation; Kalman filters; Satellite laser ranging; Laser ranging

15. NUMBER OF PAGES

37

16. PRICE CODE

17. SECURITY CLASSIFICATION OF REPORT	18. SECURITY CLASSIFICATION OF THIS PAGE	19. SECURITY CLASSIFICATION OF ABSTRACT	20. LIMITATION OF ABSTRACT
Unclassified	Unclassified	Unclassified	